Continuous health monitoring of asphalt concrete pavements using surface-mounted battery-free wireless sensors

Conference Paper · June 2017

DOI: 10.1201/9781315100333-93

4 authors, including:

Hassene Hasni
Michigan State University
35 PUBLICATIONS **533** CITATIONS

SEE PROFILE

Amir H. Alavi
University of Pittsburgh
208 PUBLICATIONS **10,816** CITATIONS

SEE PROFILE

Karim Chatti
Michigan State University
122 PUBLICATIONS **1,164** CITATIONS

SEE PROFILE

Continuous Health Monitoring of Asphalt Concrete Pavements Using Surface-Mounted Battery-Free Wireless Sensors

H. Hasni, A.H. Alavi, K. Chatti & N. Lajnef
Department of Civil and Environmental Engineering, Michigan State University, East Lansing, MI 48824, USA

ABSTRACT: This paper presents a new surface sensing approach for health monitoring of asphalt concrete (AC) pavements utilizing a new class of self-powered wireless sensors. The proposed method was based on the interpretation of the data stored in the memory gates of the sensor. A three-dimensional finite element analysis was performed to obtain the dynamic strain at the surface of the pavement for different damage scenarios. Damage states were defined using the element weakening method. The sensor output data was generated from the time-history of the surface strains. Thereafter, the sensor data was fitted to a Gaussian mixture model (GMM) in order to define an initial damage indicator features. Finally, probabilistic neural network classification scheme was used to classify the damage states. The results indicate that the proposed method is effective in detecting and classifying bottom-up cracks in AC pavements using a surface-mounted network of sensors.

1 INTROUCTION

Pavement health monitoring is an emerging field in pavement engineering for continuous damage assessment and safety evaluation of the pavement infrastructure system. Distresses concentrated in the asphalt concrete layer can lead to the failure of the pavement structure over time. Bottom-up fatigue cracking is one of the main failure modes in asphalt concrete (AC) pavements. The fatigue life of pavements is mainly related to the nature and the amplitude of the applied loading (Miller and Belliger, 2003). A realistic modeling of the dynamic loading as well as the pavements layers material properties are essential to provide accurate predictions of the mechanical response of the structure. Previous studies were conducted to analyze the effect of the analysis type on the pavement response. A dynamic analysis may increase the fatigue damage and rutting damage by 4 times and at least 40 % respectively (Cebon, 1986). Furthermore, other researchers showed that the dynamic response of the pavement is usually higher than the response given by a quasi-static analysis. Static analysis may results in about 39% difference on the tensile strain compared to a transient dynamic analysis (Yoo and Al-Qadi, 2007). Furthermore, hot-mix asphalt (HMA) behaves as a viscoelastic materials and highly depends on both loading frequency and temperature. From a sensing perspective, strain gages and traditional wired sensors for pavement health monitoring are widely used to detect variations of the strain amplitude due to the pavement deterioration (Dong et al., 2012; Xue, 2013; Lajnef et al., 2013; Yang et al., 2014).

A major drawback of these methods is that they need precise individual placement, wiring systems and external power supply. To cope with these limitations, recent development in the field of pavement health monitoring has revealed the capabilities of the wireless sensors networks (WSN) in detecting damage in pavement structures (Chatti et al., 2016). A new class of self-powered wireless sensors (SWS) is developed by authors at Michigan State University (MSU) (Alavi et al., 2016a-b; Alavi et al., 2017). The advantage of this new sensing technology is that the sensor is harvesting the micro-strain energy of the host structure under mechanical excitation via a piezoelectric transducer. This type of materials can be used to transform a mechanical loading into an electrical charge using the direct piezoelectric effect process. The generated electricity is used to empower the sensor and asses the health state of the structure. A prototype of the sensor is shown in Figure 1. The sensor has seven memory gates that cumulatively record the voltage/strain droppage over time (Figure 1(a)). Figure 1(b) is the interface board of the sensor and Figure 1(c) is the sensor electronics part. The communication between the sensor and a servi-

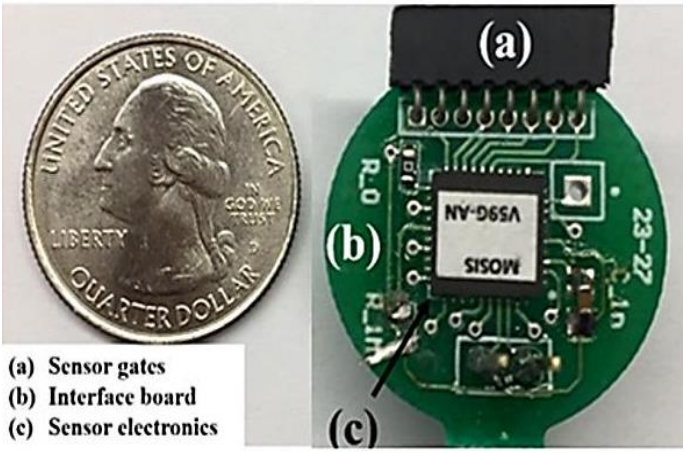

Figure 1. Prototype of the SWS.

ce vehicle could be effectuated using a Radio Frequency Identification (RFID) scanner to read the data stored on board the memory cells of the sensor. Previous studies on the self-powered wireless sensor showed that cracks in pavement could be detected based on the interpretation of the data of a constant injection rate class of SWS (Chatti et al., 2016). In their study, the SWS was embedded inside the asphalt layer. However, the device could be damaged and their replacement might be expensive. Therefore, placing the sensors network near the top surface of the pavement seems to be an attractive solution. In addition, for the case of a constant injection rate SWS, the data can be fitted to a cumulative density function (CDF). However, in this paper, each gate of the sensor has a specific injection rate, which makes the interpretation of the data more complicated.

This study proposes a new method for pavement health monitoring based on a surface sensing approach. The proposed detection mechanism is based on integrating the finite element method (FEM) and probabilistic neural networks (PNN). Intensive finite element (FE) analysis of a moving load on a pavement section was performed to obtain a realistic response. The proposed method uses features extracted from the sensors output distributions to define initial damage indicators. Thereafter, the extracted features from the WSN were fused to increase the classification accuracy.

2 SMART SENSOR AND PROPOSED DAMAGE DETECTION SYSTEM

The smart sensor is capable of continuously monitoring the strain events within the host structure. As mentioned before, the memory cells records the cumulative drop of voltage/strain at a preselected threshold level.

A schematic representation of the working principle of the sensor is presented in Figure 2. Figure 2(a) represents the input signal and Figure 2(b) displays the output of the sensor.

The recorded strain droppage is a function of the cumulative time intersections and the gates injection rates as follow:

$$S_j = S_0 - I_{gj} \times \sum_{j=1:7} T_i^j \quad (1)$$

Where S_j is the sensor strain at gate j, T_i^j is the duration of time intersection number i at the preselected threshold j (see Figure 2), and I_{gj} is the injection rate of gate j. The injection rates are property of the sensors and they control the strain/voltage droppage rates over time.

As seen in Figure 2, there is a considerable loss of the sensed information because the data is compressed as a function of the cumulative time. Therefore, a statistical method was proposed to extract valuable features from the sensor distribution. In this paper, the output histogram is fitted to a Gaussian mixture model. GMMs are powerful tools to describe many types of data.

The probability density function (PDF) of a Gaussian mixture (GM) distribution is given by the following expression:

$$p(x) = \sum_{k=1}^{M} \frac{c_k}{\sqrt{2\,\pi\,{\sigma_k}^2}} \exp\left[-\frac{1}{2}\left(\frac{x-\mu_k}{\sigma_k}\right)^2\right] \quad (2)$$

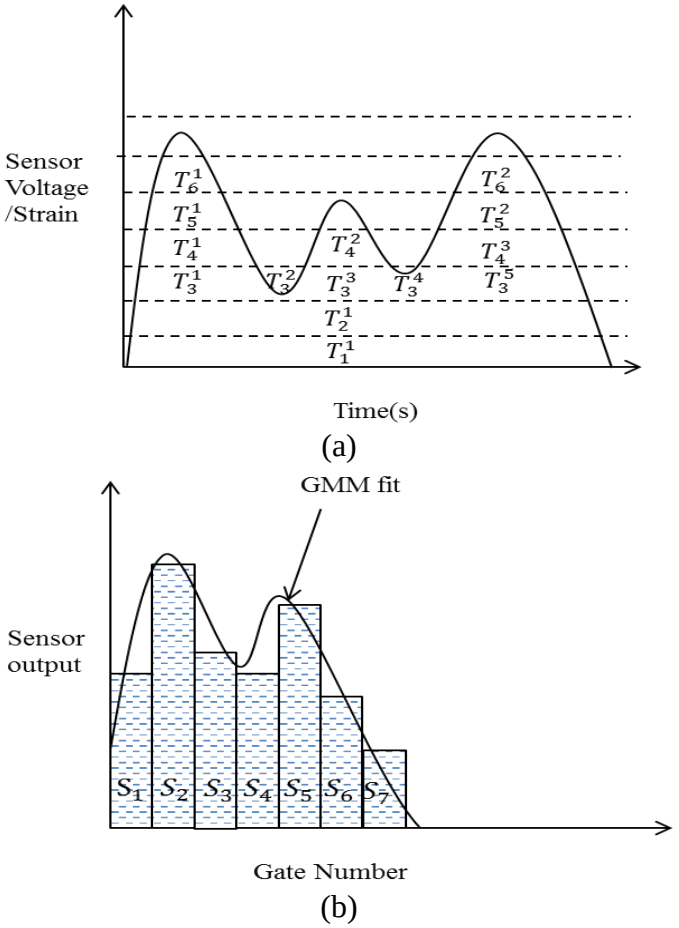

Figure 2. Procedure of obtaining the sensor output histogram.

where: $(\mu_k, \sigma_k, k = 1..M)$ are mixture component parameters (mean and standard deviation) and c_k ae the mixture weights. The mixture weights of the PDF should satisfy the following condition:

$$\sum_{k=1}^{M} c_k = 1 \quad (3)$$

In this paper, the strain droppage histogram was fitted by a bimodal (M=2) GMM as follows:

$$\Delta\varepsilon(g) = (\sum_{j=1}^{7} \Delta\varepsilon_j) \sum_{k=1}^{2} \frac{\alpha_k}{\sqrt{2\,\pi\,\sigma_k{}^2}} \exp\left[-\frac{1}{2}\left(\frac{g-\mu_k}{\sigma_k}\right)^2\right] \quad (4)$$

where g is the gate number, (μ_k, σ_k) are the mixture component parameters, α_k is a parameter that represents the mixture weights and $\Delta\varepsilon_j$ is the cumulative droppage of strain at gate number j (j=1..7).
The GMM parameters (μ_k, σ_k) can be regarded as damage indicators as they represent the only viable tools to characterize the SWS data. Furthermore, the strain response of the pavement changes with damage progression in the structure. Therefore, based on the relative variation of the strain, the GMM parameters will change according to the damage growth. Consequently, the damage is logically considered a function of (μ_k, σ_k). This will be shown below.

In this paper, the damage detection procedure is divided into three major phases: (1) Structural simulations of the targeted structure, (2) extraction of preliminary damage indicator features, and (3) damage detection and classification based on fusing the sensors network data. The last step is achieved through an artificial intelligence (AI) approach.
For the analysis, the initial strain value of each memory gate was set to S_0 = 500 $\mu\varepsilon$. The gate injection rates as well as the strain threshold levels are displayed in Table 1.

Table 1. The preselected strain levels and the gate injection rates considered for the analysis.

Gate number	Strain threshold level $(\mu\varepsilon)$	Injection Rates $(\mu\varepsilon/s)$
1	80	0.001000
2	100	0.005710
3	120	0.023162
4	140	0.027822
5	160	0.006562
6	180	0.005989
7	200	0.032792

3 FINITE ELEMENT MODEL

3.1 *FE model description*

The FE simulations were performed using ABAQUS (ABAQUS, 2010). The element weakening method (EWM) was used to introduce the damage to the pavement. A total of 13 damage states were introduced to the pavement including different combinations of the reduced AC modulus and the damage zone height. The damage zone was assumed to have a rectangular parallelepiped shape of 120 × 120 × h mm. The parameter h denotes the height of the damage zone which is variable in the analysis. The damaged AC volume was located at the center bottom of the AC layer. The modulus of the damaged zone was reduced to 30%, 50%, 70%, and 90% from the instantaneous modulus of the AC layer. The damage heights (h) were 20 mm, 40 mm, and 60 mm.

The damage states are displayed in Table 2. Figure 3 shows the damage location, cross section of the pavement, and the measurement locations.
The load contact area was assumed to be rectangular (19.43 × 13.38 cm). The tire pressure was 862 kPa and the vehicle speed was 67 mph (30 m/s).
An implicit dynamic analysis was selected for the analysis. In order to simulate the moving load at the desired speed, a FORTRAN code was developed to define the DLOAD subroutine in ABAQUS.

Table 2. Damage scenarios.

Damage class	Damage height (mm)	Reduction in modulus (%)
C0	0	0
C1	20	30
C2	20	50
C3	20	70
C4	20	90
C5	40	30
C6	40	50
C7	40	70
C8	40	90
C9	60	30
C10	60	50
C11	60	70
C12	60	90

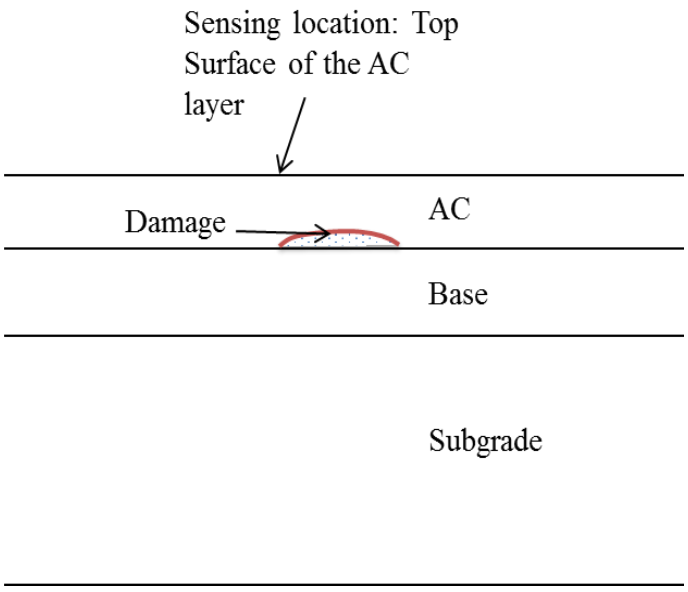

Figure 3. A schematic description of the damage and the measurement locations.

The time increment was set to 0.001 s, and therefore, the loading progresses by 30 mm (30 m/s × 0.001) during one time step.

The sensors were placed at the surface of the AC layer. Up to 32 sensing nodes were used to measure the strain changes due to damage progression. The network of sensors is displayed in Figure 4.

The pavements layers were modeled using different material properties. The AC layer had viscoelastic properties while the base and subgrade were assumed to behave as a linear elastic material. A 5 % damping ratio was defined for the base and subgrade layers.

The pavement model was meshed using two different types of elements: eight-node linear brick elements with reduced integration (C3D8R) and eight node linear infinite elements (CIN3D8). The infinite elements were used to minimize the reflection of the shear and dilatational waves back into the FE mesh. The loaded strip as well as the location of the infinite elements are shown in Figure 5.

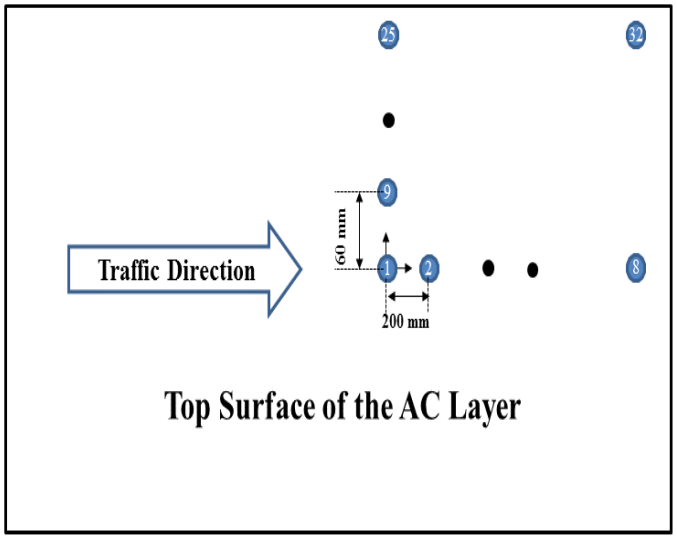

Figure 4. Sensors locations.

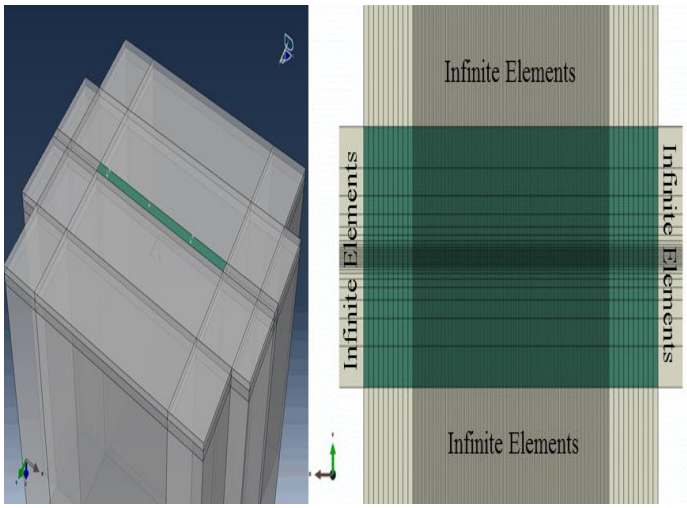

Figure 5. Loading path and FE model mesh.

3.2 *FE results*

Figure 6 shows the time history of the first principal strain (in absolute value) at the location of sensor 1 for the C0 (intact), C4, C8 and C12 damage classes. Figure 7 displays the results of the FE analysis for different damage heights and modulus reductions at sensors locations 1 and 25.

As it seen in Figure 6, the amplitude of the maximum principal strain increases with damage progression. Furthermore, the strain amplitude continuously increases between damage classes at sensor 1 location (Figure 7(a)). However, the behavior is inverted for sensor 25. This sensor is located at an offset of 180 mm from the longitudinal direction (parallel to the traffic direction).

It can be concluded that when the sensor is located along the wheel path, the strain increases with damage progression, however, an offset with respect to

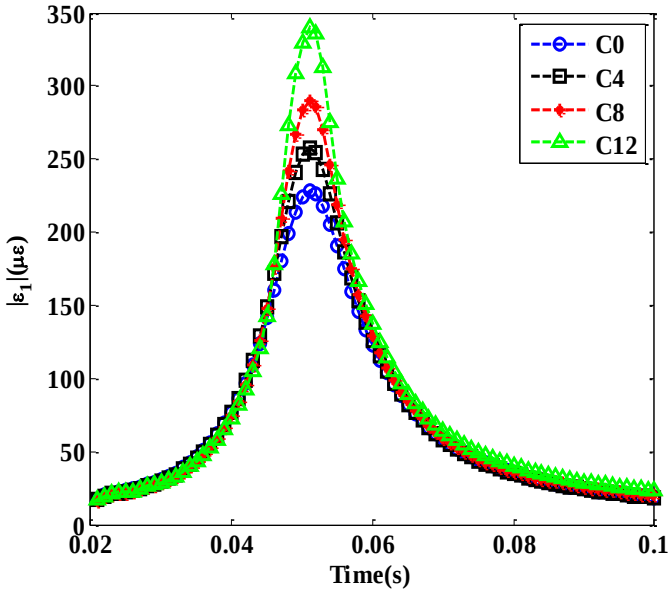

Figure 6. Strain history of sensor 1 for the intact, C4, C8 and C12 damage classes.

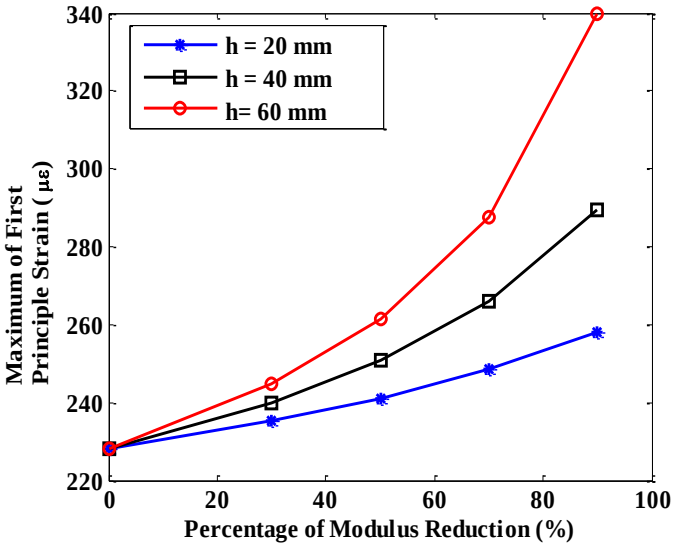

(a)

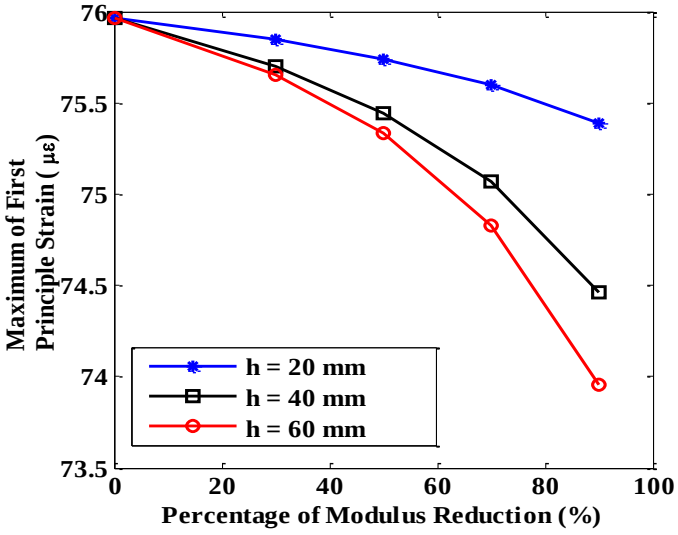

(b)

Figure 7. Maximum principal strain vs percentage of modulus reduction for different damage heights at sensor location: (a) 1 and (b) 25.

the longitudinal direction could create a different behavior of the strain amplitudes trends as a function of the damage evolution in the structure as shown in Figure 7(b).

4 DAMAGE DETECTION RESULTS

4.1 *Individual sensing results*

After obtaining the FE results, the sensor output was generated as discussed in section 2. Thereafter, the histograms of all the sensors were fitted to a GMM distribution in order to obtain an initial damage indictor features (μ_k, σ_k) , $k = 1,2$. Figure 8 displays the GMM fit to sensor 1data for the intact and the C12 damage states.

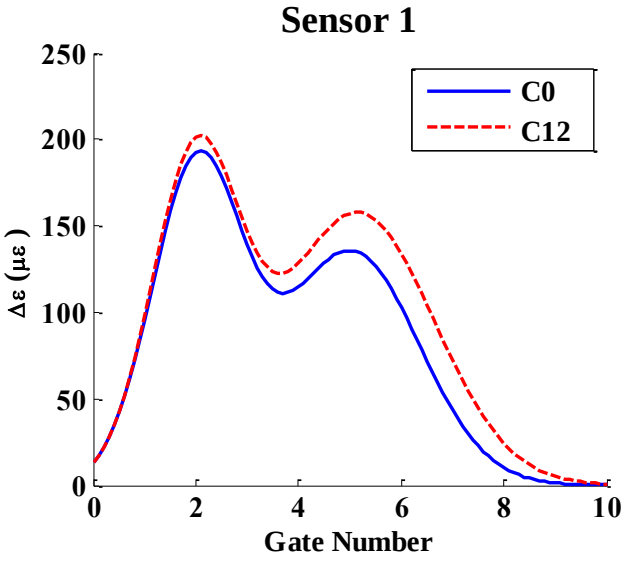

Figure 8. GMM fit to sensor 1 data for the intact and C12 damage classes.

As it can be seen in the figure, the mean (μ_1) of the first components of the GMM shifts to the left (decreases) and the second mean μ_2 shifts to the right (increases). In addition, the standard deviations σ_1 and σ_2 increase with damage progression as the distribution expands. Therefore, the GMM components seems to be a good indicators of damage progression. Thus, the damage could be defined as follow:

$$\text{Damage} = \text{function}\,(\mu_1, \mu_2, \sigma_1, \sigma_2) \tag{5}$$

However, if a sensor is located far from the damage zone, the amplitude of the strain does not change remarkably between damage classes, and therefore, the sensor histogram outputs become very similar. As a consequence, the GMM parameters (initial damage predictors) also become very close and the damage classes cannot be separated. On the other hand, when the sensor is located at certain offset from the traffic direction, the strain might decrease with damage progression. In this case, the GMM parameters can detect the damage event but it cannot estimate its severity (the damage class). In order to overcome these issues, a data fusion model was proposed based on the 'sensor group effect'.

4.2 *Data fusion model*

In this section, the initial damage indicator features of all the sensors were fused to define a new set of damage predictors based on the group effect of a network of sensors concept. If a sensor is located far from the damage zone, the group effect of the sensors network will help to increase its sensitivity to the damage growth. The new features were proposed as follow:

$$\underline{y} = \begin{cases} y_1 = \frac{x_1 - x_{1\text{ave}}}{x_{1\text{STD}}} \\ y_2 = \frac{x_2 - x_{2\text{ave}}}{x_{2\text{STD}}} \\ y_3 = \frac{x_3 - x_{3\text{ave}}}{x_{3\text{STD}}} \\ y_4 = \frac{x_4 - x_{4\text{ave}}}{x_{4\text{STD}}} \\ y_5 = \frac{x_1 - x_{1\text{STD}}}{x_{1\text{ave}}} \\ y_6 = \frac{x_2 - x_{2\text{STD}}}{x_{2\text{ave}}} \\ y_7 = \frac{x_3 - x_{3\text{STD}}}{x_{3\text{ave}}} \\ y_8 = \frac{x_4 - x_{4\text{STD}}}{x_{4\text{ave}}} \\ y_9 = \frac{(x_1 + x_3) - (x_{2\text{ave}} + x_{4\text{ave}})}{x_{1\text{ave}} + x_{3\text{ave}}} \\ y_{10} = \frac{(x_2 + x_4) - (x_{1\text{ave}} + x_{3\text{ave}})}{x_{2\text{ave}} + x_{4\text{ave}}} \end{cases} \tag{6}$$

where:

$$\begin{cases} x_1 = \mu_1 \\ x_2 = \sigma_1^2 \\ x_3 = \mu_2 \\ x_4 = \sigma_2^2 \end{cases} \quad (7)$$

and:

- x_i: The i[th] feature of the initial feature vector,
- $x_{i_{\text{ave}}}$: The average of x_i for all patterns corresponding to a specific damage state,
- $x_{i_{\text{STD}}}$: The standard deviation of x_i for all patterns corresponding to a specific damage state.

As indicated by Equation 6, the new input feature vector has 10 dimensions, and each components is a function of the average/standard deviation of the initial feature vector components.

Different feature selection algorithms were used to select the best set of damage predictors. The sequential forward selection (SFS), sequential backward selection (SBS), and the exhaustive search methods were performed on the new feature vectors. According to the results, the exhaustive search algorithm gives the optimal set of features that provides the best accuracy. The optimal set was found to be:

$$S_{optimal} = \{y_4, y_7, y_9\} \quad (8)$$

For the classification, 4 damage classes were defined based on the damage height as follow:
Class 1: Intact structure
Class 2: h = 20 mm
Class 3: h = 40 mm
Class 4: h = 60 mm

The detection accuracy for the training, validation and testing data are equal to 100%, 96.55% and 93.10%, respectively. Figure 9 displays the confusion matrixes. A confusion matrix is a table that describes the performance the classifier. The columns of the each matrix represents the predicted class, while each row represents the actual class.

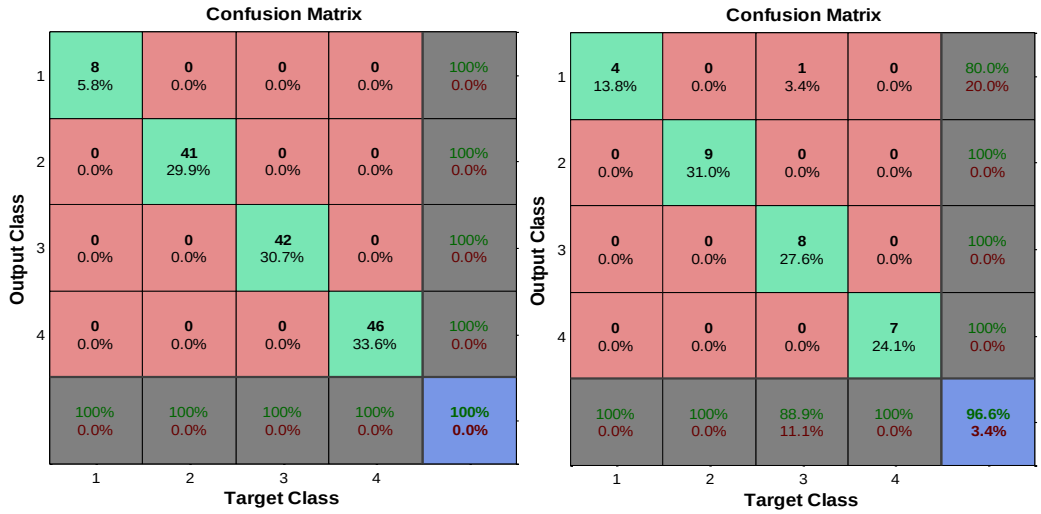

(a) Training (b) Validation

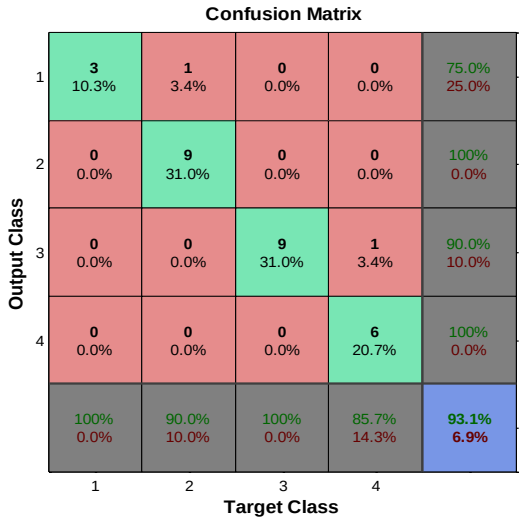

(c) Testing

Figure 9. Confusion matrixes for: (a) training, (b) validation and (c) testing.

5 CONCLUSION

This paper presents a new approach for detecting bottom-up cracking in AC pavements based on a surface sensing approach. Different numerical simulations were performed to obtain the response of the pavements under various damage scenarios. The damage was created at the bottom of the AC layer based on the reduction of its relaxation modulus and the damaged volume height. The pavement was subjected to a moving load at a highway speed. The load was created using a DLOAD subroutine developed in FORTRAN programing language. In addition, the sensor output was generated using the dynamic strain extracted from the pavement surface. Initial damage predictors were extracted from the sensor output distribution by fitting the sensor data to a GMM. Thereafter, a PNN classification scheme was applied to a data fusion model derived from the initial damage indicators in order to classify the damage states.

The following conclusions can be drawn from the results presented in this paper:

1. The amplitude of the surface strains change with damage progression.
2. The location of the sensor with respect to the damage controls the trends representing the variation of the strain amplitude with respect to the damage state (size and reduced AC modulus).
3. The bi-modal GM components are good surface indicators of damage occurrence but they are very dependent on the location of the sensor with respect to the damage location.
4. The data fusion model gives satisfactory damage detection accuracy (93.1 % on testing).

6 REFERENCES

ABAQUS, (2010). ABAQUS/CAE User's Manual Version 6.10, *Dassault Systèmes*.

Alavi, A.H., Hasni, H., Lajnef, N., Chatti, K., & Faridazar, F. (2016a). An Intelligent Structural Damage Detection Approach Based on Self-Powered Wireless Sensor Data. *Automation in Construction* 62: 24–44.

Alavi, A.H., Hasni, H., Lajnef N., Chatti K., & Faridazar F. (2016b). Damage Detection Using Self-Powered Wireless Sensor Data: An Evolutionary Approach. *Measurement* 82: 254–283.

Alavi, A. H., Hasni, H., Jiao, P., Borchani, W., & Lajnef, N. (2017). Fatigue cracking detection in steel bridge girders through a self-powered sensing concept. *Journal of Constructional Steel Research*, 128: 19-38.

Cebon, D. (1986). Road damaging effects of dynamic axle loads. In: *Proceedings of the international symposium on heavy vehicle weights and dimensions*, Kelowna, BC, Canada: 37–53.

Chatti, K., Alavi, A. H., Hasni, H., Lajnef, N., & Faridazar, F. (2016). Damage Detection in Pavement Structures Using Self-powered Sensors. In *8th RILEM International Conference on Mechanisms of Cracking and Debonding in Pavements* (pp. 665-671). Springer Netherlands.

Dong, Z. J., Li, S. L., Wen, J. Y., & Chen, H. C. (2012). Asphalt Pavement Structural Health Monitoring Utilizing FBG Sensors. *Advanced Engineering Forum*, Vol. 5, pp. 339-344.

Lajnef N., Chatti K., Chakrabartty S., Rhimi M., & Sarkar P. (2013). Smart Pavement Monitoring System. *Report: FHWA-HRT-12-072, Federal Highway Administration (FHWA)*, Ishington, DC.

Miller, J. S. & Bellinger, W. Y. (2003). Distress identification manual for long-term pavement performance program (fourth revised edition). *Report FHWA-RD-03-031, Federal Highway Administration (FHWA)*, Washington, DC.

Xue, W. (2013). Integrated Transportation Monitoring System for Both Pavement and Traffic. *PhD Thesis*, Virginia Polytechnic Institute and State University, Blacksburg, VA.

Yang, S., Ceylan H., Gopalakrishnan K., & Kim S. (2014). Smart airport pavement instrumentation and health monitoring, *Construction and Environmental Engineering Conference Presentations and Proceedings*. Paper 8.

Yoo, P.J. & Al-Qadi, I.L. (2007). Effect of transient dynamic loading on flexible pavements. *Transportation Research Record*, 1990: 129–140.